

## Monolithically integrated self-rolled-up microtube-based vertical coupler for three-dimensional photonic integration

Xin Yu, Ehsan Arbabi, Lynford L. Goddard, Xiuling Li, and Xiaogang Chen

Citation: [Applied Physics Letters](#) **107**, 031102 (2015); doi: 10.1063/1.4927243

View online: <http://dx.doi.org/10.1063/1.4927243>

View Table of Contents: <http://scitation.aip.org/content/aip/journal/apl/107/3?ver=pdfcov>

Published by the [AIP Publishing](#)

---

### Articles you may be interested in

[Vertically integrated metal-clad/silicon dioxide-shell microtube arrays for high-spatial-resolution light stimuli in saline](#)

Appl. Phys. Lett. **104**, 164101 (2014); 10.1063/1.4871710

[On-chip intra- and inter-layer grating couplers for three-dimensional integration of silicon photonics](#)

Appl. Phys. Lett. **102**, 211109 (2013); 10.1063/1.4808208

[Monolithically integrated low-loss silicon photonic wires and three-dimensional tapered couplers fabricated by self-profile transformation](#)

Appl. Phys. Lett. **91**, 191114 (2007); 10.1063/1.2809359

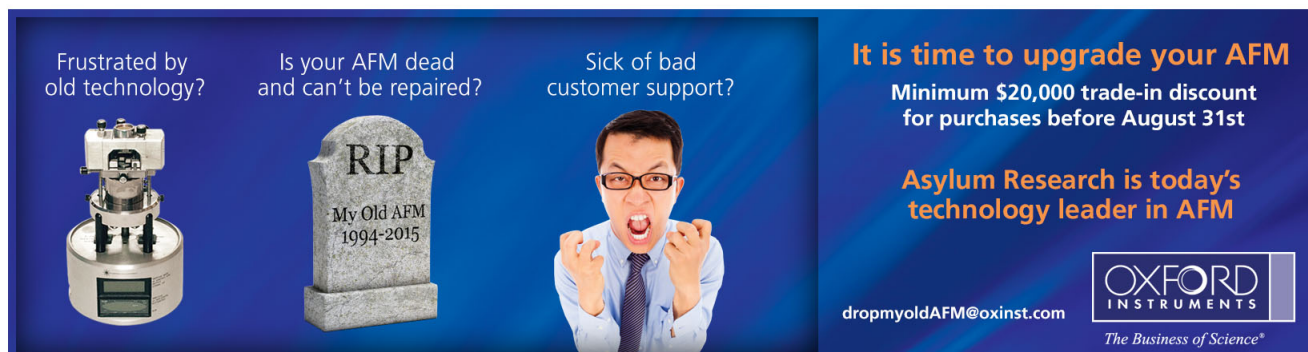
[High performance asymmetric graded index coupler with integrated lens for high index waveguides](#)

Appl. Phys. Lett. **90**, 201116 (2007); 10.1063/1.2740589

[Three-dimensional integration of metal-oxide-semiconductor transistor with subterranean photonics in silicon](#)

Appl. Phys. Lett. **88**, 121108 (2006); 10.1063/1.2184754

---



Frustrated by old technology?

Is your AFM dead and can't be repaired?

Sick of bad customer support?

**It is time to upgrade your AFM**

Minimum \$20,000 trade-in discount for purchases before August 31st

Asylum Research is today's technology leader in AFM

[dropmyoldAFM@oxinst.com](mailto:dropmyoldAFM@oxinst.com)

**OXFORD**  
INSTRUMENTS  
*The Business of Science®*

# Monolithically integrated self-rolled-up microtube-based vertical coupler for three-dimensional photonic integration

Xin Yu, Ehsan Arbabi,<sup>a)</sup> Lynford L. Goddard, Xiuling Li, and Xiaogang Chen<sup>b)</sup>

*Department of Electrical and Computer Engineering, University of Illinois, Urbana, Illinois 61801, USA*

(Received 4 May 2015; accepted 8 July 2015; published online 20 July 2015)

We demonstrate a self-rolled-up microtube-based vertical photonic coupler monolithically integrated on top of a ridge waveguide to achieve three-dimensional (3D) photonic integration. The fabrication process is fully compatible with standard planar silicon processing technology. Strong light coupling between the vertical coupler and the ridge waveguide was observed experimentally, which may provide an alternative route for 3D heterogeneous photonic integration. The highest extinction ratio observed in the transmission spectrum passing through the ridge waveguide was 23 dB. © 2015 AIP Publishing LLC. [<http://dx.doi.org/10.1063/1.4927243>]

Photonic integrated circuits (PICs) are widely considered to be the future technology that may provide viable solutions to many technical obstacles currently faced by the semiconductor industry. As micro- and nano-electronic technology gradually loses the momentum to keep the development pace predicted by Moore's law, integrated nanophotonics is positioned to solve some of the imperative issues such as ultra-high bandwidth and extremely low energy dissipation for on-chip signal processing and transmission. A chip-wise photonic communication system, or sometimes called a photonic Computer system,<sup>1</sup> requires monolithically integrated active and passive photonic devices to achieve ultra-compactness, unprecedented data transmission rate, minimal insertion loss, high coupling efficiency, ultra-low power dissipation, and deeply reduced packaging cost. Current state-of-the-art photonic integration technology focuses on building the photonic interconnection system in a planar or two-dimensional (2D) platform. However, due to the incompatibility of the material systems and fabrication processes for the active and the passive components, 2D photonic integration either may not be able to provide the necessary system performance or may demand significant modification to the existing fabrication infrastructure, which translates to much higher cost.

Historically, there are two material platforms being developed separately to serve different application needs in PICs. The compound semiconductor material platform, which contains III–V and/or II–VI compounds and their alloys, is mainly used for active photonic devices such as semiconductor lasers and light emitting diodes (LEDs) because of the direct band-gap and the capability for band engineering. Silicon has emerged as the preferred platform for passive photonic devices, thanks to the tremendous advancement in silicon fabrication technology. But, the indirect band-gap in silicon prevents it from being an efficient light emitter. The fabrication processes of these two material platforms are generally not compatible with each other

especially in mass-production. Methods to integrate active and passive photonic devices on the same chip to achieve heterogeneous integration have been a technical challenge ever since the 1960s. Three-dimensional (3D) photonic integration is expected to provide an elegant solution to such a long-standing challenge by allowing both active and passive photonic elements to be optimized and fabricated on their own device planes, and then to be coupled together three-dimensionally by efficient vertical couplers at predefined strategic locations.

Research efforts to extend the 2D planar integration into all three dimensions dated back to 1990s.<sup>2</sup> The vertically stacked directional coupler (VSDC) is currently the most widely used coupling device between two adjacent photonic device planes.<sup>2–5</sup> However, this type of coupler suffers from some fundamental limitations that prevent it from being an ideal vertical coupler for heterogeneous 3D photonic integration. First, the VSDC requires that both of the participating waveguides are located close to each other, e.g., within a fraction of the wavelength of the propagating light, typically less than 250 nm, so that the evanescent coupling can take place. If the separation between these two adjacent device planes is uniform, accidental evanescent coupling between components on different device planes is unavoidable, which will result in cross talk and extra channel noise, and in turn, degrade the system performance. If the separation is not uniform, the fabrication process becomes prohibitively complicated. Second, the two arms of a VSDC consume the real estate in their corresponding device plane, which is always a scarce resource for the integrated system. Finally, the quality factor of directional coupler based switch is generally poorer as compared to resonator based ones.

In this paper, we present an efficient vertical photonic coupler based on self-rolled-up silicon nitride ( $\text{SiN}_x$ ) tubular membranes, which is monolithically integrated with a  $\text{Si}_3\text{N}_4$  ridge waveguides to achieve 3D photonic coupling. The self-rolled-up microtube (also called the tube waveguide in photonic applications) is formed using a strain-engineered double-layer membrane patterned on a planar substrate using standard 2D processing technology and self-assembled into a 3D structure after being selectively released and driven by mismatched strain between the two layers.<sup>6</sup> Tremendous

<sup>a)</sup>Present address: Department of Electrical Engineering, California Institute of Technology, Pasadena, California 91125, USA.

<sup>b)</sup>Author to whom correspondence should be addressed. Electronic mail: [oxgchen@illinois.edu](mailto:oxgchen@illinois.edu).

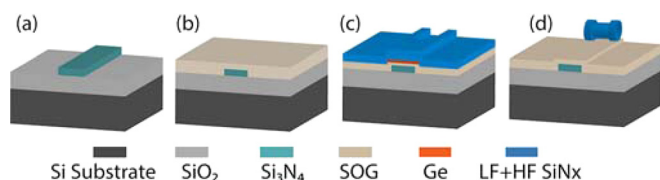


FIG. 1. Schematic of the fabrication processes to monolithically integrate the self-rolled-up tube vertical coupler to a ridge waveguide: (a) Si<sub>3</sub>N<sub>4</sub>/SiO<sub>2</sub> ridge waveguide; (b) planarization by SOG; (c) tube pattern definition by lithography and SiN<sub>x</sub> bilayer deposition; and (d) sacrificial layer removal and tube formation.

progress has been made in recent years on precisely controlling the self-rolling process to achieve the desired microtube structure, which found broad applications from advanced microelectronics to photonics to intelligent synthetic neural circuits.<sup>7–10</sup> The tube waveguide has been demonstrated both theoretically and experimentally to support whispering gallery modes (WGM) circulating along its circumference.<sup>6,11–26</sup> The light can be evanescently coupled between the tube and a straight waveguide once their separation is made adequately small, typically within a fraction of the wavelength of the propagating light. Several research groups have already demonstrated 3D photonic integration using the tube waveguide.<sup>11,20,24,26</sup> However, a monolithically integrated version of the tube waveguide to a planar ridge waveguide coupling has not yet been demonstrated experimentally. The result we report here is a monolithically integrated resonator-based vertical photonic coupler on silicon platform. It could potentially serve as a cornerstone for further development of tube waveguide based 3D heterogeneously integrated PIC systems.

In this paragraph, we outline the major fabrication steps involved in achieving the monolithic 3D photonic integration of the self-rolled-up tube coupler and the ridge waveguide underneath it. The substrate was a (100) p-type silicon substrate from Rogue Valley Microdevices. It contains a 6 μm

thermal SiO<sub>2</sub> and a 150 nm Si<sub>3</sub>N<sub>4</sub> layer formed by low-pressure chemical vapor deposition (LPCVD). The ridge waveguides were formed by electron beam (E-beam) lithography and reactive ion etching (RIE), as shown in Fig. 1(a). In our experiment, all waveguides have a uniform height of 150 nm and their widths vary from 2 to 5 μm. To facilitate tube formation, we have to planarize the sample surface after etching the waveguides. This was achieved by covering the ridge waveguides with a layer of spin-on glass (SOG) thicker than the height of the ridge waveguides and then etching back the SOG by RIE leaving about 100 nm on top of the waveguides, as shown in Fig. 1(b). The thickness of the SOG residual layer, which can be precisely controlled, is one parameter that allows us to adjust the coupling gap between the tube couplers and the ridge waveguides. After planarization, a 20 nm sacrificial layer of germanium (Ge) was deposited by electron beam evaporation, and the tube patterns were defined by traditional photolithography and RIE down to the SOG layer as shown in Fig. 1(c). Subsequently, a 60 nm strained SiN<sub>x</sub> bilayer was deposited by dual-frequency plasma enhanced chemical vapor deposition (PECVD) to cover the entire sample. The bilayer is composed of a 30 nm layer of 380 kHz low frequency (LF) SiN<sub>x</sub> and a 30 nm layer of 13.56 MHz high frequency (HF) SiN<sub>x</sub>. The residual stress of the LF and HF SiN<sub>x</sub> thin film was –900 MPa and +300 MPa, respectively.<sup>8</sup> In order for the SiN<sub>x</sub> bilayer to be lifted up from the sacrificial layer and scrolled into a tube directionally, a window down to the Ge layer was opened by photolithography and RIE from one side of tube pattern. Once Ge was removed by the etchant (H<sub>2</sub>O<sub>2</sub>) from this window, the SiN<sub>x</sub> lifted up from the substrate; dynamic coherent tearing occurred at two sides and the multi-turn spiral tubular SiN<sub>x</sub> structure was formed, as shown in Fig. 1(d). We should emphasize that all of these fabrication steps are fully compatible with standard planar silicon processing techniques.

The fabricated 3D integrated tube coupler and ridge waveguides are shown in Fig. 2. Figure 2(a) shows the cross-

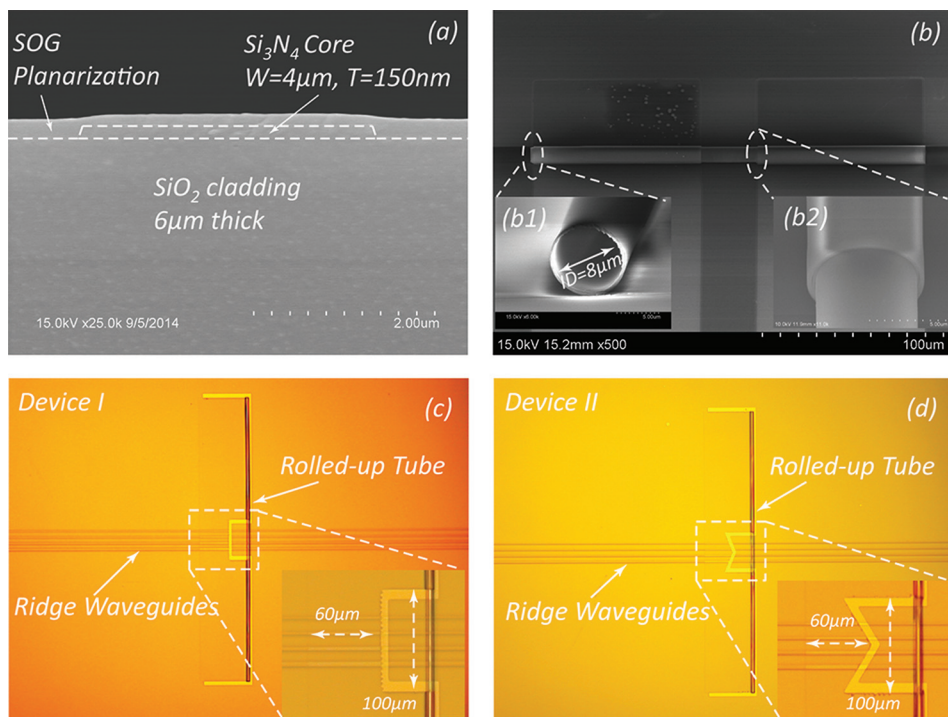


FIG. 2. SEM and optical images of the monolithically integrated tube resonator with ridge waveguide. (a) Si<sub>3</sub>N<sub>4</sub> ridge waveguide after planarization by SOG and (b) the self-rolled-up tube resonator, inset (b1) shows the enlarged cross-sectional view of the tube at one end, inset (b2) shows the top view of the connection section between the center tube waveguide and the supporting pedals. (c) and (d) Microscopy images of the top view of self-rolled-up tubes integrated with ridge waveguides. Devices I and II contain different axial patterns in the coupling section.

sectional view of the substrate interface near a ridge waveguide after planarization. It can be seen that the flatness at the top of the SOG layer is much improved; the height of the small bump directly above the ridge waveguide is only about 50–70 nm, which is sufficiently small to ensure the continuity of the SiN<sub>x</sub> bilayer membrane when it is lifted up. In Fig. 2(b), one may notice that the 2D pattern of self-rolled-up tube has two arms extended on each side of the main coupling section. After tube rolling stops, these two extended arms form extra layers of tube wall on both sides of the coupling section. Such a structure provides two desired features for the vertical coupler. First, by controlling the length of the extended arms, we can precisely determine how high the center coupling section is elevated from the SOG layer, which is the second method allowing us to fine-tune the coupling distance between the tube and the waveguide beneath it as shown in Fig. 2(b2). Second, because the extra turns of tube pedestal will result in a small change of the effective refractive index of the azimuthal mode, the two pedestals act as weak reflectors to provide some axial confinement for the electromagnetic field inside the tube waveguide. The inner diameter of the tube is 8 μm, which is decided by the thickness, Young's modulus, and residual stress of SiN<sub>x</sub> bilayer. We can obtain different diameters simply by adjusting the SiN<sub>x</sub> thickness or the residual stress of the bilayer.<sup>8</sup> Figures 2(c) and 2(d) show the optical microscope images of the self-rolled-up tube directly fabricated on a series of ridge waveguides with different widths, varying from 2 to 5 μm and spaced equally by 15 μm. As shown in the insets, the rolling distance and axial length of both tubes are 60 μm and 100 μm, respectively, which are determined by the width and the length of the SiN<sub>x</sub> patterns. These two devices are fabricated on the same substrate and processed together. Therefore, based on the 8 μm inner diameter, there is about 2 coiled turns of the tube, and total wall thickness is 120 nm. There are two more turns of the pedestal on both sides so the central tube coupler is suspended 120 nm above the planarized surface. The primary difference between these two devices is the fine patterns in the central coupling section of the original 2D SiN<sub>x</sub> membrane. The triangle patterns in device II are introduced to enhance the axial mode confinement of the tube waveguide.

The coupling efficiency between the monolithic integrated tube coupler and the ridge waveguide was

investigated by measuring the waveguide transmission spectra. Figure 3 shows a schematic of the experimental setup. The light source is a Hewlett Packard 8168C tunable laser source, which has an output wavelength range from 1480 nm to 1580 nm. The laser output passes through an optical isolator, a polarization controller, and a polarizer to ensure that the input light is linearly polarized. Unlike the 2D ring resonator based coupler that typically uses TM polarized light, the vertical tube coupler is more efficient by using TE polarized light. A fiber splitter is used to get a small fraction of the input light for reference; the remaining light is coupled into and collected from the ridge waveguide using fibers tapered in a wedge shape to create an elliptical beam for good coupling into the rectangular waveguide cross-section. The transmitted light passes through an optical coupler and is sent to a photo-detector and an optical power meter. The reflected light was measured using an optical circulator and another photo-detector. The average transmission of an 8 mm ridge waveguide including the two fiber to waveguide coupling interfaces is measured to be about -8.5 dB as shown in Fig. 4 (black curve). The coupling loss per facet is typically 4.0 dB. Therefore, the linear propagation loss of the ridge waveguide is about 0.6 dB/cm.

Figure 4 shows the experimentally measured transmission spectra for the ridge waveguide and the waveguide coupled with the vertical tube coupler. The blue and the red curves illustrate the transmission spectra of devices I and II shown in Figs. 2(c) and 2(d), respectively. The black curve is the transmission spectrum of a stand-alone ridge waveguide without the vertical tube coupler above it fabricated on the same substrate at the same time, which is shown as a benchmark. The ridge waveguides in all three cases have the same width (4 μm) and height (150 nm). Critical coupling between the ridge waveguide and the tube coupler can be clearly identified at discrete wavelengths. The highest extinction ratio is found to be about 23 dB at 1558 nm for device II, which is an order of magnitude higher than those observed in non-monolithically integrated tube to waveguide coupling experiments.<sup>11,20</sup> Compared to the free space coupling between a tube and two suspended optical fibers reported in Ref. 10 and the tapered fiber aided pick-up and place method reported in Ref. 20, the monolithically integrated vertical tube coupler to ridge waveguide scheme provides much more accurate control of the coupling distance to realize the desired critical

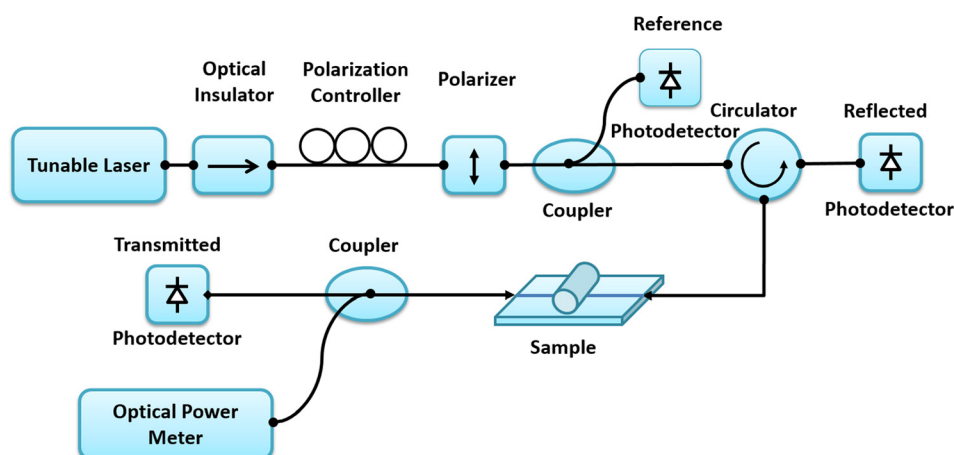


FIG. 3. Schematic of the setup for measuring the transmission spectra of the tube resonators. OI: optical isolator, PC: polarization controller, OP: optical polarizer, PD: photodetector, and DUT: device under test.

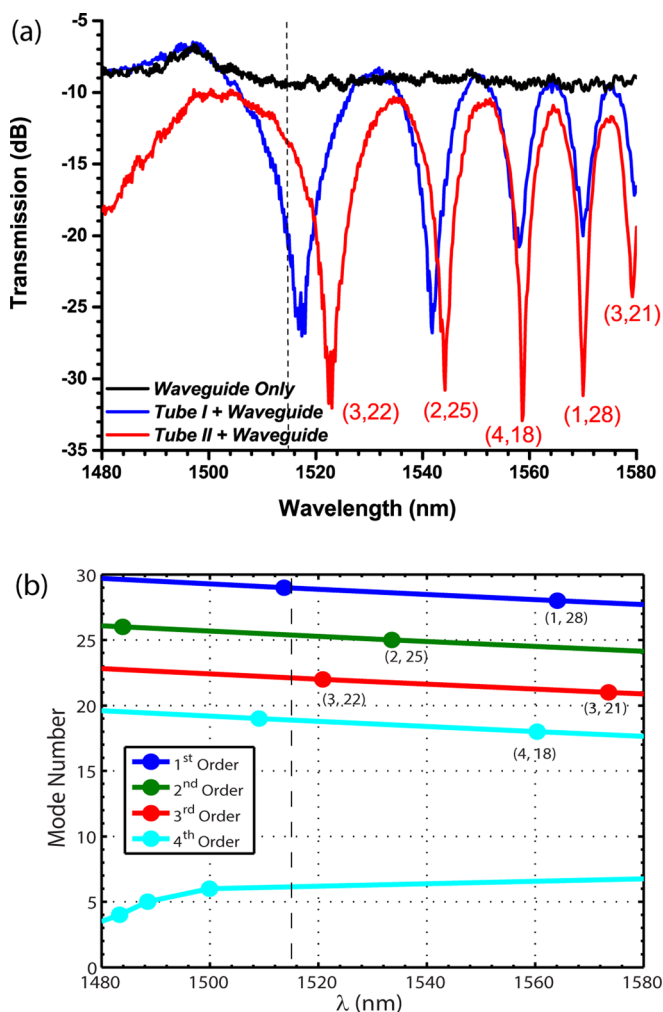


FIG. 4. (a) Transmission spectra of the waveguide only (black), the device I (blue), and the device II (red). In all three cases, the waveguides have the same width ( $4\ \mu\text{m}$ ) and height ( $150\ \text{nm}$ ). Devices I and II are those shown in Figs. 2(c) and 2(d), respectively. The only difference between these devices is the axial pattern, which provides different axial confinements to the tube coupler. (b) Theoretically calculated resonant modes of the first 4 orders within the same spectral range. The modes are labeled as  $(m,n)$  in both figures, where  $m$  is the order of the mode and  $n$  is the mode number.

coupling. The spectral locations of the resonant peaks are slightly shifted between devices I and II. This is likely due to the different axial confinements the light experiences when it is coupled into the tube. In contrast to a typical photoluminescence (PL) experiment, even with axial confinement in device II, the number of resonance peaks did not appear to increase. This could be explained as following: first, the triangle pattern only provided weak axial confinement; second, unlike PL experiment which all modes supported by the microtube can be excited by strong external source, in the vertical coupling experiment efficient coupling only took place while the propagation constant of the WGM inside the microtube matched with that of the ridge waveguide mode. Fig. 4(b) shows the theoretically calculated resonant modes of the first 4 orders using a conformal transformation based analytical model reported in Ref. 27, which captures the non-concentric nature of the microtube and takes only the refractive indices and geometric parameters such as the diameter, single layer thickness, and number of turns of the microtube as inputs. Using a refractive index of 1.98 for the tube and an

inner diameter of  $7.9\ \mu\text{m}$ , the simulation results agreed well with the experimental values. It can be seen from Fig. 4(b) that for the 4th order azimuthal mode, the resonant wavelength does not increase monotonically with decreasing mode number when the mode number is small, which are the modes with majority of the mode energy being confined within the hollow core region of the microtube. There are several such modes folded back to the spectral region that we are interested in. Particularly, there are 6 modes of different orders crammed between 1480 and 1515 nm (on the left side of the dashed line shown in Fig. 4). The coupling between the waveguide mode and these modes is the reason that there is no steep transmission valley for the wavelength below 1515 nm. On the contrary, the modes with resonant wavelength above 1515 nm are well separated. We can clearly identify 5 resonant modes between 1515 nm and 1580 nm from the transmission spectrum, which match with the theoretical prediction. We noticed that the exact spectral locations of the theoretically predicted resonant modes are shifted with respect to the experimentally measured ones. This discrepancy can be attributed to the assumptions that we made to simplify the simulation. We assume an infinitely long tube with invariant cross-sectional structure along the rotating axis of the tube, so that we may ignore the field component along this axis and reduce the 3D problem to a 2D problem. The tubes we used in the experiment have finite length and have fine features introduced to provide axial confinement. In reality, the axial component of the field cannot be ignored. The measured resonant modes are superpositions of the azimuthal component and axial component of the field, which are phase matched with the waveguide mode. Therefore, it is not too surprising to observe a spectral shift.

In this paper, we presented an experimental demonstration of a monolithically integrated vertical photonic coupler based on  $\text{SiN}_x$  self-rolled-up tubes with a  $\text{Si}_3\text{N}_4$  ridge waveguide. The fabrication process is fully compatible with standard and prevailing planar silicon processing technology. Strong light coupling between the ridge waveguide and the vertical coupler was observed. The extinction ratio is an order of magnitude higher than non-integrated tube and waveguide coupling. This vertical coupler opens a new avenue to achieve monolithic 3D photonic integration. Potentially, it can be used to couple light between two photonic device planes: the passive silicon photonic plane mainly handling light transmission, switching and detection, and the active electro-optical device plane fabricated using compound semiconductor materials to provide efficient light source and other electro-optical modulation functionalities. Such a 3D photonic integration may give system designers the freedom to separately build the active and the passive photonic devices in the materials that best suit the application and then couple them together three dimensionally. On the other hand, this approach allows industry to utilize optimized results from decades of research and investment in both material platforms. Furthermore, such a 3D PIC system can be seamlessly integrated with the current state-of-the-art electronic integrated system to realize advanced functionalities and system performance.

This work was supported in part by the Strategic Research Initiative Program from the College of Engineering

at the University of Illinois at Urbana-Champaign and by NSF CAREER Award No. ECCS-1055941 with matching funds from the University of Illinois. X.L. acknowledges financial support by the U.S. Department of Energy, Office of Basic Energy Sciences, Division of Materials Sciences and Engineering under Award No. DE-FG02-07ER46471.

- <sup>1</sup>Y. A. Vlasov, *IEEE Commun. Mag.* **50**(2), s67 (2012).
- <sup>2</sup>B. Liu, A. Shakouri, P. Abraham, and J. E. Bowers, *Electron. Lett.* **35**(18), 1552 (1999).
- <sup>3</sup>B. Liu, A. Shakouri, P. Abraham, and J. E. Bowers, *IEEE Photonics Technol. Lett.* **12**(4), 410 (2000).
- <sup>4</sup>N. Sherwood-Droz and M. Lipson, *Opt. Express* **19**(18), 17758 (2011).
- <sup>5</sup>K. Preston, B. Schmidt, and M. Lipson, *Opt. Express* **15**(25), 17283 (2007).
- <sup>6</sup>X. L. Li, *J. Phys. D: Appl. Phys.* **41**(19), 193001 (2008).
- <sup>7</sup>P. Froeter, Y. Huang, O. V. Cangelaris, W. Huang, E. W. Dent, M. U. Gillette, J. C. Williams, and X. L. Li, *ACS Nano* **8**(11), 11108 (2014).
- <sup>8</sup>W. Huang, S. Koric, X. Yu, K. J. Hsia, and X. Li, *Nano Lett.* **14**(11), 6293 (2014).
- <sup>9</sup>P. Froeter, X. Yu, W. Huang, F. Du, M. Y. Li, I. Chun, S. H. Kim, K. J. Hsia, J. A. Rogers, and X. L. Li, *Nanotechnology* **24**(47), 475301 (2013).
- <sup>10</sup>X. Yu, W. Huang, M. Y. Li, T. M. Comberiate, S. B. Gong, J. E. Schutt-Aine, and X. L. Li, *Sci. Rep.* **5**, 9661 (2015).
- <sup>11</sup>S. Böttner, S. Li, M. R. Jorgensen, and O. G. Schmidt, *Appl. Phys. Lett.* **102**(25), 251119 (2013).
- <sup>12</sup>S. Böttner, S. L. Li, J. Trommer, S. Kiravittaya, and O. G. Schmidt, *Opt. Lett.* **37**(24), 5136 (2012).
- <sup>13</sup>V. A. B. Quinones, G. S. Huang, J. D. Plumhof, S. Kiravittaya, A. Rastelli, Y. F. Mei, and O. G. Schmidt, *Opt. Lett.* **34**(15), 2345 (2009).
- <sup>14</sup>G. S. Huang, S. Kiravittaya, V. A. Bolaños Quiñones, F. Ding, M. Benyoucef, A. Rastelli, Y. F. Mei, and O. G. Schmidt, *Appl. Phys. Lett.* **94**(14), 141901 (2009).
- <sup>15</sup>C. Strelow, C. M. Schultz, H. Rehberg, M. Sauer, H. Welsch, A. Stemmann, C. Heyn, D. Heitmann, and T. Kipp, *Phys. Rev. B* **85**(15), 155329 (2012).
- <sup>16</sup>C. Strelow, H. Rehberg, C. M. Schultz, H. Welsch, C. Heyn, D. Heitmann, and T. Kipp, *Physica E* **40**(6), 1836 (2008).
- <sup>17</sup>Ch. Strelow, H. Rehberg, C. M. Schultz, H. Welsch, Ch. Heyn, D. Heitmann, and T. Kipp, *Phys. Rev. Lett.* **101**(12), 127403 (2008).
- <sup>18</sup>C. Strelow, C. M. Schultz, H. Rehberg, H. Welsch, C. Heyn, D. Heitmann, and T. Kipp, *Phys. Rev. B* **76**(4), 045303 (2007).
- <sup>19</sup>T. Kipp, H. Welsch, C. Strelow, C. Heyn, and D. Heitmann, *Phys. Rev. Lett.* **96**(7), 077403 (2006).
- <sup>20</sup>Z. B. Tian, V. Veerasubramanian, P. Bianucci, S. Mukherjee, Z. T. Mi, A. G. Kirk, and D. V. Plant, *Opt. Express* **19**(13), 12164 (2011).
- <sup>21</sup>F. Li, S. Vicknesh, and Z. Mi, *Electron. Lett.* **45**(12), 645 (2009).
- <sup>22</sup>X. L. Li, *Adv. Opt. Photonics* **3**(4), 366 (2011).
- <sup>23</sup>I. S. Chun, K. Bassett, A. Challa, and X. L. Li, *Appl. Phys. Lett.* **96**(25), 251106 (2010).
- <sup>24</sup>S. Bhowmick, T. Frost, and P. Bhattacharya, *Opt. Lett.* **38**(10), 1685 (2013).
- <sup>25</sup>M. H. T. Dastjerdi, M. Djavid, and Z. Mi, *Appl. Phys. Lett.* **106**(2), 021114 (2015).
- <sup>26</sup>Q. H. Zhong, Z. B. Tian, V. Veerasubramanian, M. H. T. Dastjerdi, Z. T. Mi, and D. V. Plant, *Opt. Lett.* **39**(9), 2699 (2014).
- <sup>27</sup>X. G. Chen, *Opt. Express* **22**(13), 16363 (2014).